On the correlation of Young's modulus and the fracture strength of metallic glasses

C. C. Yuan and X. K. Xi[a)]
Institute of Physics, Chinese Academy of Sciences, Beijing 100190, China

(Received 29 September 2010; accepted 9 December 2010; published online 8 February 2011)

It is generally believed that there is no simple relationship between ultimate fracture strength and stiffness for an elastically isotropic material. By taking bulk metallic glasses (BMGs) as model materials, the relation between ultimate fracture strength and elastic moduli was analyzed within Griffith theory framework. The observed correlation between elastic moduli and fracture strength in BMGs reveals the effects of BMG defects and plastic zone size on the crack resistance of these model materials. © *2011 American Institute of Physics*. [doi:10.1063/1.3544202]

Bulk metallic glasses (BMGs) are of great technological and fundamental importance because of their high strength, large elastic limit, high toughness, and because of other unique properties.[1] It is generally believed that there is no simple relationship between ultimate tensile strength and stiffness for an elastically isotropic material.[2] The reason is that when a conventional material fails under stress, defects determine its strength while it is not the case for elastic modulus which is a fundamental property. It is of importance to know if BMGs without the complication of different crystal structures,[3] show clear relationship between strength and elastic modulus. Extensive work on this issue has been done by many researchers.[4,5] A clear correlation between Young's modulus and fracture strength has been found in metallic glasses,[6,7] which was described by the fact that metallic glasses have nearly the same elastic strain ~2%. The underlying physics or how to understand this characteristic still remains to be unclear.[3,8] In this work, we show that the correlation can be simply understood based on the extension of Griffith theory.

Griffith initially considered a semi-infinite microcrack of length "2*c*" in an ideal glass under mode I tensile loading conditions. As the stress reaches a critical level, many of these microcracks then intersect before the glass fails along a shear zone. A constant energy per unit area, equal to $2\gamma_s$ of forming two fresh fracture surfaces, is then released from the elastic fields. The fracture strength of brittle materials can be determined:[9]

$$\sigma_f = \sqrt{2E\gamma_s/\pi c}, \tag{1}$$

where "*c*" is Griffith-like flaw size. Orowan and Irwin later considered a local plastic zone of crack tip in quasi-brittle materials and introduced plastic work energy. For quasibrittle BMGs showing marginal plastic strain, fracture strength,[10,11]

$$\sigma_f = \sqrt{\frac{E(2\gamma_s + \gamma_p)}{\pi C}}, \tag{2}$$

where "*C*" refers to the plastic zone size instead of pre-crack size in Orowan–Irwin's equation;[10] γ_p is the plastic work energy mostly consumed in the vicinity of the crack tip, here K_C is fracture toughness which is defined as $\sqrt{E(2\gamma_s+\gamma_p)/\pi}$. γ_p is much larger than γ_s and equal to $\sim 1000\gamma_s$ for quasibrittle materials,[10] so $(E\gamma_p/\pi) \approx K_C^2$.

However, from Eqs. (1) and (2), the linear relation of materials strength to Young's modulus is not straightforward. Fracture surface energy γ_s actually can be determined by $\gamma_s = kEd$;[12] here d is the lattice constant for crystalline materials while it is the statistical average of inter-atomic distance on the first coordination shell for glasses, ~2.6–3.0 Å; k is a constant that depends on local stress-strain function selected for the materials. Thus in brittle metallic glasses, we get, $\sigma = \sqrt{2kd/\pi cE}$ by substitution of γ_s. "Griffith cracks" refers to the largest cavities between solute centered clusters resulting from the coalescence of excess free volumes.[13,14] These cavities are akin to Bernal canonical holes in dense random packing. The Griffith-crack size ($2c$) can be expected to be proportional to the average outer diameter of the associated clusters since the coalescence of such Bernal holes might be extremely limited in response to the shear stress induced dilatation within shear bands. The average outer diameter of these solute centered clusters has been taken to be approximately three times the diameter of the atoms of the base element in the glasses based on the efficient dense random packing model.[15] c can thus be thought to be proportional to d in brittle metallic glass. For quasibrittle BMGs, previous work shows that plastic zone size, C is proportional to the dimplelike size (w) on the crack surfaces for typical metallic glasses.[16] Figure 1 shows that K_C^2/E^2 follows a linear relationship with "w" for typical BMGs and the slope yields a constant, 0.013 ± 0.001. This means γ_p/w is proportional to E since $K_C^2 = (E\gamma_p/\pi)$ by assuming $\gamma_p \gg \gamma_s$. Since C is proportional to w,[16] then γ_p/C should also be proportional to E. A linear relationship between fracture strength and Young's modulus can thus be expected in metallic glasses.

Figure 2 shows the relationship of Young's modulus (E) with fracture strength (σ_f) for ~60 typical BMGs and other materials for comparison. For the large variety of materials under quasi-static loading conditions, the ratio σ/E is about 1/10 for ideal materials without defects, ~1/50 for metallic glasses, and ~1/100 for ductile crystalline metals. Young's

[a)]Electronic mail: xi@iphy.ac.cn.

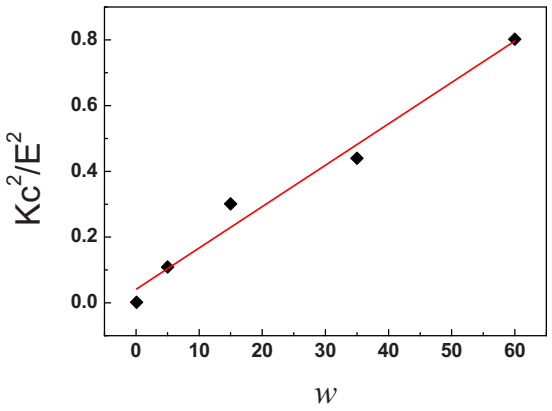

FIG. 1. (Color online) A plot of K_c^2/E^2 against dimplelike structure size of w on fracture surfaces of typical BMGs. The data are from Table I. The solid line is linear least square root fitting. The slope is 0.013 ± 0.001.

modulus (E) is obtained by ultrasonic measurement. Here, ultimate compressive strength has been adopted instead of ultimate tensile strength from the following considerations: (1) the experimental data for the former quantity are plentiful while the data for the latter are quite scarce;[17,18] (2) Griffith theory framework has been successfully applied to predict the uniaxial compressive fracture stress of brittle materials;[19] (3) little asymmetry of tensile/compressive strength have been obtained and the ratio is within a narrow range of 0.8–1.0 for various metallic glasses.[7,20] This symmetry originates from the characteristic shear banding deformation and fracture mechanisms of these materials. The normal stress plays a less significant role in comparison with shear stress,[20,21] which can be corroborated by the observations that ultimate fracture strength is insensitive to the applied hydrostatic pressure. The data in Fig. 2 are collected from Refs. 18 and 22–30. The data of some typical glasses are listed in Table I. From Fig. 2 and Table I, the relation of fracture strength of BMGs with their Young's moduli follows a similar scaling behavior to crystalline metals and oxide glasses, that is, $\sigma_f = k'E$ but with a different coefficient, that is $k' = \sim 1/50$. This $\sigma \sim E/50$ linear relationship clearly makes BMGs distinct from other materials. From Fig. 2, the dimensionless constant, $k' = \sim 1/50$ seems to be applicable for all metallic

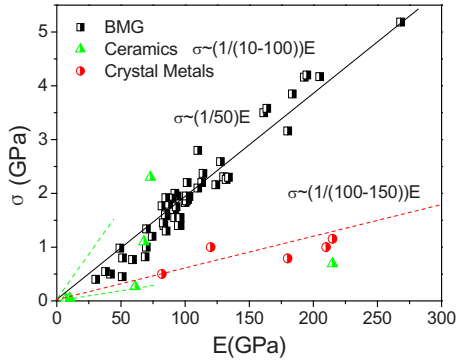

FIG. 2. (Color online) The ultimate fracture strengths (σ_f) vs Young's modulus (E) of various BMGs tested under room temperature. The data of conventional crystalline alloys and ceramics are also shown for comparison. References are within the context. The solid line is linear least square root fitting. The slope is 0.0213 ± 0.0007.

glasses, which means metallic glasses follow a similar underlying mechanism of deformation and fracture. A plausible structural origin of this common mechanism of metallic glasses might originate from their characteristic local atomic structure and interatomic bonding character.

As shown above, $\sigma_f = \sim E/50$ can be applied for BMGs in general. After close observation, however, there is some small but observable nonlinearity or scatter. For brittle BMGs, the measured fracture strength randomly distributed around $\sigma = k'E$, while the strength of tough BMGs showing marginal plasticity tends to be smaller than that is expected from $\sigma_f = E/50$. To understand this scattering, it is worth noting here that fracture strength, σ_f, is a complex material parameter which could be influenced by both intrinsic parameters such as inter-atomic interaction, detailed structure such as defects and their interactions, fracture and deformation mode, and extrinsic factors such as preparation, loading conditions, specimen size and aspect ratio geometry, and so on, while it is not the case for Young's modulus which is mainly determined by pair interaction $V(r)$ between ions in solids.[31] We propose that these scattering can be classified as two categories: one is random in nature which is due to the flaw size distribution, while the other one is systematic in nature which is caused by an enhanced fracture process zone size.

For brittle materials, the fracture stress and its fluctuation can be described by the equation: $\sigma_f = \sqrt{(2E\gamma_s/\pi(c+\xi))}$, where $|\zeta|$ is the fluctuation of flaw size c due to various preparation conditions. This effect of flaw size fluctuation on fracture strength should be random in nature and thereafter strength fluctuations can be described by Weibull statistical distribution which agrees well with experiments.[32] When $|\xi/c|$ is small, the fluctuation of strength will be expected to be negligible. A recent study clearly shows that the strength of a Zr-based BMG indeed follows a Weibull statistical distribution with a small fluctuation.[32] If $|\xi/c|$ is large, however, the fluctuation could be huge and the measured materials fracture strength will never reach its intrinsic value, which is also the case for some other very brittle materials such as ceramic glass and some oxide glass.

When large plastic work energy dissipation is involved in the fracture of tough materials, according to Eq. (2), these tough materials become insensitive to flaw size c when $C \gg c$. For crystalline solids, crack tip blunting will hinder crack extension by emitting dislocations and/or branching. These processes will dissipate most fracture energy. However, for amorphous alloys, stress concentration at crack tip will be relieved through a different mechanism, such as athermal shear transformation zone activation,[33,34] which is the carrier of plasticity and it will yield energy dissipation in the vicinity of crack tip. The plastic deformation and fracture events are thus controlled by this irreversible energy dissipation process.[35,36] Since fracture energy is mostly dissipated through plastic work, while $\gamma_p = (K_{IC}^2/E(1-\nu^2))$ (Refs. 37 and 38) (under plane strain condition, where ν is Poisson's ratio), that means γ_p is proportional to plastic process zone size (C).[39] Further, the size of characteristic dimple like vein pattern obtained from scanning electron microscope (SEM) fracture morphology has also been linked to fracture energy,

TABLE I. Fracture strength (σ_f), Young's modulus (E), calculated surface energy (γ_s), and stress intensity factor (K_C) for typical metallic glasses. Crystalline alloys and ceramic are also listed for comparison.

Materials	σ_f (GPa)	E (GPa)	γ_s [a] (J m^{-2})	K_C [b] (MPa m$^{1/2}$)
BMGs[c]				
$Zr_{41.25}Ti_{13.75}Cu_{12.5}Ni_{10}Be_{22.5}$[d] (295 K, 1×10^{-4} s^{-1})	1.86	96	1.47	86
$Zr_{41.25}Ti_{13.75}Cu_{12.5}Ni_{10}Be_{22.5}$[d] (523 K, 1×10^{-4} s^{-1})	1.68	96	1.47	
$Zr_{55}Cu_{35}Al_{10}$(298 K)[e]	1.74	83	1.36	
$Zr_{55}Cu_{35}Al_{10}$(77 K)[e]	2.02	83	1.36	
$Pd_{77.5}Si_{16.5}Cu_6$	1.55	92.9	1.38	51
$Cu_{60}Zr_{20}Hf_{10}Ti_{10}$	1.95	101	1.41	67
$Ce_{70}Al_{10}Ni_{10}Cu_{10}$	0.4	30.3	0.92	10
$Mg_{65}Cu_{25}Tb_{10}$	0.8	51.3	0.76	2
$Fe_{30}Co_{30}Ni_{15}Si_8B_{17}$[f]	2.8	110	1.64	
$Co_{43}Fe_{20}Ta_{5.5}B_{31.5}$ (as-cast)[g]	5.185	268	1.63	
$Co_{43}Fe_{20}Ta_{5.5}B_{31.5}$ (annealed)[g]	5.334	268	1.63	
Crystalline metals[h]				
Cast irons	0.350–1.000	165–180		22–54
High carbon steels	0.550–1.640	200–215		27–92
Stainless steels	0.480–2.240	189–210		62–280
Aluminum alloys	0.058–0.550	68–82		22–35
Titanium alloys	0.300–1.625	90–120		14–120
Ceramics[h]				
Borosilicate glass	0.264–0.384	61–64		0.5–0.7
Silica glass	1.100–2.300	68–74		0.6–0.8
Brick	0.050–0.140	10–50		1–2
Stone	0.034–0.248	6.9–21		0.7–1.5
Alumina	0.690–5.500	215–413		3.3–4.8

[a]Reference 42.
[b]Reference 38.
[c]References 22–24.
[d]Reference 25.
[e]References 26 and 27.
[f]Reference 28.
[g]Reference 29.
[h]Reference 30.

showing the size of dimplelike structure is proportional to C in metallic glasses.[16] That means γ_p dissipates in the vicinity of crack tip of metallic glasses at different length scales, and the total energy release rate is primarily controlled by the ratio of γ_p/C. According to Eq. (2), material fracture strength from both γ_p and γ_s contributions will be $\sigma_f = \sqrt{E(2\gamma_s+\gamma_p)/\pi C}$. C ranges from nanometer to micrometer length scales for metallic glasses,[16] while γ_s changes only a factor of 1 to 2 for most metals when cracking. This means the partial contribution from γ_s to strength is underweighted since γ_s is a material property which is weakly dependent on fracture process zone size when crack starts propagating.[40] Above all, surface energy dissipation within plastic zone

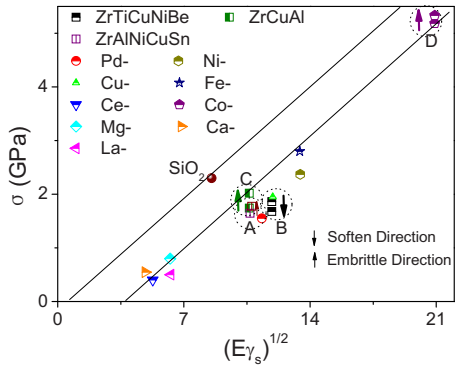

FIG. 3. (Color online) The ultimate fracture strengths (σ_f) vs square root of Young's modulus and surface energy ($\sqrt{E\gamma_s}$) for ten metallic glasses systems. The data are from Table I. The slope corresponds to the size of fracture process zone.

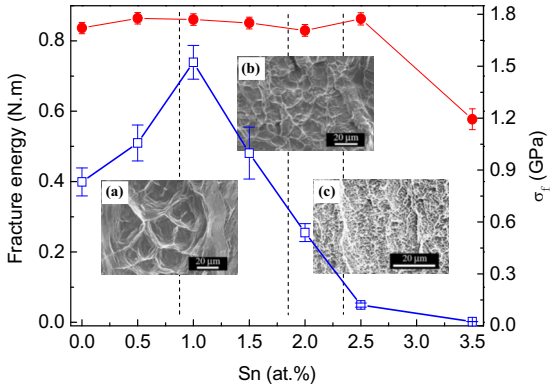

FIG. 4. (Color online) The fracture energy (G_f) (hole square) and ultimate fracture strengths (σ_f) (solid circle) as a function of Sn concentration in $Zr_{61}Cu_{18.3-x}Ni_{12.8}Al_{7.9}Sn_x$ ($0<=x<=3.5$) BMGs. The inset shows the structural evolution of crack surfaces accompanying DBT with the addition of Sn, (a) x=1.0; (b) x=2.0; (c) x=2.5.

TABLE II. Elastic constants (Young's modulus, E; bulk modulus, B; and shear modulus, G), Poisson's ratio (ν), density (ρ), fracture strength (σ_f), dimple size measured on fracture surface (w), fracture energy (G_f) integrated from three-point bending stress-strain curves, and calculated fracture surface energy (γ_s) for $Zr_{61}Cu_{18.3-x}Ni_{12.8}Al_{7.9}Sn_x$ ($0<=x<=2.5$) BMGs.

BMGs	σ_f (GPa)	E (GPa)	B (GPa)	G (GPa)	ν	ρ (g cm^{-3})	w (μm)	Fracture energy (G_f) (N m)	γ_s[a] (J m^{-2})
$Zr_{61}Cu_{18.3}Ni_{12.8}Al_{7.9}$	1.721	79.11	101.38	28.87	0.3699	6.797	20	0.399	1.441
$Zr_{61}Cu_{17.8}Ni_{12.8}Al_{7.9}Sn_{0.5}$	1.777	78.81	101.28	28.76	0.3703	6.788	30	0.510	1.443
$Zr_{61}Cu_{17.3}Ni_{12.8}Al_{7.9}Sn_1$	1.770	77.44	102.55	28.18	0.3741	6.805	35	0.739	1.434
$Zr_{61}Cu_{16.8}Ni_{12.8}Al_{7.9}Sn_{1.5}$	1.750	77.25	92.95	28.37	0.3615	6.815	30	0.481	1.430
$Zr_{61}Cu_{16.3}Ni_{12.8}Al_{7.9}Sn_2$	1.707	81.92	99.81	30.05	0.3632	6.765	10	0.255	1.426
$Zr_{61}Cu_{15.8}Ni_{12.8}Al_{7.9}Sn_{2.5}$	1.774	81.47	102.14	29.8	0.3671	6.818	1	0.049	1.423

[a]Reference 42.

plays a key role of the deviation from the linear scaling of strength with respect to moduli data, which is manifested as the deviation on the $\sigma-\sqrt{E\gamma_s}$ curve, as shown clearly in Fig. 3. Here, the abscissa E is replaced by square root of elastic moduli and γ_s, which is calculated by atomic ratio mixing up surface energy of pure elements.[41,42] To avoid surface segregation effects, the BMGs containing the elements Bi, C, and P are not included.[41]

The above extension of Griffith model might provide insights in designing BMG materials with tuned ultimate fracture strength and plasticity. $Zr_{61}Cu_{18.3-x}Ni_{12.8}Al_{7.9}Sn_x$ ($0<=x<=3.5$) BMG system were selected to verify our above analysis. This alloy system is interesting since it shows ductile to brittle transition (DBT) upon minor Sn alloying.[43] It is well known that fractography has been used with fracture mechanics to understand the causes of fracture and also verify the theoretical predictions. The DBT occurs in this system when Sn content is above 1%. Then this DBT can be simply characterized by the evolution of fractography and by the sharp change in fracture energy under three-point bending experiments, as shown in Fig. 4. Typical SEM fracture morphologies were also included in Fig. 4. Dimple size w and fracture energy G_f are all listed in Table II. Cleary, the dimple size increases upon Sn addition when Sn<1 at. %, reaches maximum when Sn is around 1 at. %, while decrease sharply when Sn concentration is beyond 2.5 at. %. From Fig. 4, it can be seen that fracture energy follows a similar behavior to fracture morphologies upon Sn alloying, indicating plastic process zone acts as a toughening mechanism for this type of materials. Further, the ratio of $\sigma_f/\sqrt{E\gamma_s}$ correlates with plastic zone size and hence plasticity since toughness enhances plasticity for all modes of loading, which clearly illuminates the intrinsic connection of data deviation on the curve of $\sigma_f-\sqrt{E\gamma_s}$, see point A in Fig. 3. When Sn concentration is beyond 2.5 at. %, the sharp drop of strength indicate the material becomes brittle and sensitive to the embedded cracks or flaws which are close or even larger than the plastic zone size C. The correlation of $\sigma_f/\sqrt{E\gamma_s}$ with plastic zone size C and plasticity can also be found in other BMGs. In ZrCuNiAlSn BMGs, from the stress-strain curves, the decrease in $\sigma_f/\sqrt{E\gamma_s}$ correlates well with plasticity[44] and vice versa, reminiscent of the well-known fact that improving plasticity while sacrificing strength in low temperature tempering of martensitic steel. The correlation of $\sigma_f/\sqrt{E\gamma_s}$ with plasticity also exists in the BMG specimen measured at different temperatures. For $Zr_{41.25}Ti_{13.75}Cu_{12.5}Ni_{10}Be_{22.5}$ compressed at 523 K under quasistatic condition, the ratio of $\sigma_f/\sqrt{E\gamma_s}$ becomes smaller while plastic strain becomes larger than room temperature[25] (see point B in Fig. 3). For $Zr_{55}Cu_{35}Al_{10}$ at low temperatures,[26] the ratio becomes larger while plastic strain becomes less, as shown at the point C in Fig. 3. After annealing below T_g for a short time even if no nanocrystal appear, $Co_{43}Fe_{20}Ta_{5.5}B_{31.5}$ BMGs becomes more brittle and the above correlation still holds, showing less deviation after annealing treatment (see the point D in Fig. 3). Considering above analysis and experimental evidences, it can be concluded that large plasticity could be obtained in BMGs by decreasing fracture strength through microstructure engineering on different length scales.[1,45,46]

There are other relevant aspects of the fracture mechanics and other models of the fracture energy dissipation.[47,48] Our arguments on the role of plastic energy are not intended to exclude these possibilities. We hope the above efforts to understand the observation we report here will provide a test of the various competing theoretical models of fracture mechanism. For instance, Griffith approach ignores the specific features of failure processes in the zone near crack tip but concentrates on the variation in energy during crack growth, a rigorous explanation of the microfracture mechanism responsible for the relevant fracture energy is worthy of a focused separate study.

In conclusion, the $\sigma\sim E/50$ scaling behavior of BMGs can be illuminated in virtue of the extension of Griffith theory. Furthermore, the recently addressed scattering[18] can also be explained within Griffith theory framework. This understanding also provides a new insight of recent experimental observations, including sample size effects on the plastic flow and fracture behaviors of BMGs.

This work was supported by the Chinese Academy of Sciences, NSF of China (Grant Nos. 50921091 and 51071171) and the National Basic Research Program of China (MOST 973, Grant No. 2010CB731600). The discussion with W. H. Wang is acknowledged.

[1]Y. H. Liu, G. Wang, R. J. Wang, D. Q. Zhao, M. X. Pan, and W. H. Wang, Science **315**, 1385 (2007).
[2]M. F. Ashby, *Materials Selection in Mechanical Design*, 3rd ed. (Butterworth-Heinemann, Oxford, 2005).
[3]A. L. Greer, Mater. Today **12**, 14 (2009).
[4]T. Masumoto and R. Maddin, Mater. Sci. Eng. **19**, 1 (1975).

[5]J. J. Gilman, J. Appl. Phys. **46**, 1625 (1975).
[6]W. H. Wang, J. Non-Cryst. Solids **351**, 1481 (2005).
[7]C. A. Pampillo, J. Mater. Sci. **10**, 1194 (1975); H. Q. Li, C. Fan, K. X. Tao, H. Choo, and P. K. Liaw, Adv. Mater. **18**, 752 (2006); Y. J. Huang, J. Shen, J. F. Sun, and Z. F. Zhang, Mater. Sci. Eng. **A498**, 203 (2008); S. Takayama and R. Maddin, Philos. Mag. **32**, 457 (1975).
[8]H. S. Chen, Rep. Prog. Phys. **43**, 353 (1980).
[9]A. A. Griffith, Philos. Trans. R. Soc. London, Ser. A **221**, 163 (1921).
[10]E. Orowan, Rep. Prog. Phys. **12**, 185 (1949).
[11]J. A. Kies, A. M. Sullivan, and G. R. Irwin, J. Appl. Phys. **21**, 716 (1950).
[12]J. J. Mecholsky, Mater. Lett. **60**, 2485 (2006); S. W. Freiman, *Fracture resistance testing of monolithic and composite brittle materials* (ASTM STP, West Conshohocken, PA, 2002) Vol. 1409, p. 17.
[13]J. Li, Z. L. Wang, and T. C. Hufnagel, Phys. Rev. B **65**, 144201 (2002).
[14]C. A. Schuh, T. C. Hufnagel, and U. Ramamurty, Acta Mater. **55**, 4067 (2007).
[15]Y. Zhang and A. L. Greer, Appl. Phys. Lett. **89**, 071907 (2006).
[16]X. K. Xi, D. Q. Zhao, M. X. Pan, W. H. Wang, Y. Wu, and J. J. Lewandowski, Phys. Rev. Lett. **94**, 125510 (2005).
[17]Y. Yokoyama, K. Fujita, A. R. Yavari, and A. Inoue, Philos. Mag. Lett. **89**, 322 (2009).
[18]W. L. Johnson and K. Samwer, Phys. Rev. Lett. **95**, 195501 (2005).
[19]W. F. Brace and E. G. Bombolakis, J. Geophys. Res. **68**, 3709 (1963).
[20]H. Kimura and T. Masumoto, Acta Metall. **28**, 1663 (1980).
[21]J. J. Lewandowski, and P. Lowhaphandu, Philos. Mag. A **82**, 3427 (2002).
[22]A. Inoue, Acta Mater. **48**, 279 (2000).
[23]W. H. Wang, C. Dong, and C. H. Shek, Mater. Sci. Eng. R. **44**, 45 (2004).
[24]W. H. Wang, J. Appl. Phys. **99**, 093506 (2006).
[25]J. Lu, G. Ravichandran, and W. L. Johnson, Acta Mater. **51**, 3429 (2003).
[26]C. Fan, P. K. Liaw, V. Haas, J. J. Wall, H. Choo, A. Inoue, and C. T. Liu, Phys. Rev. B **74**, 014205 (2006).
[27]Y. Yokoyama, T. Yamasaki, P. K. Liaw, and A. Inoue, Acta Mater. **56**, 6097 (2008).
[28]T. Zhang and A. Inoue, Mater. Trans. **42**, 1015 (2001).
[29]A. Inoue, B. L. Shen, H. Koshiba, H. Kato, and A. R. Yavari, Acta Mater. **52**, 1631 (2004).
[30]W. Martienssen and H. Warlimont, *Springer Handbook of Condensed Matter and Materials Data* (Springer, Berlin, 2005), pp. 161–559.
[31]T. Rouxel, J. Am. Ceram. Soc. **90**, 3019 (2007).
[32]H. B. Yu, W. H. Wang, J. L. Zhang, C. H. Shek, and H. Y. Bai, Adv. Eng. Mater. **11**, 370 (2009).
[33]F. Spaepen, Acta Metall. **23**, 615 (1975); A. S. Argon, *ibid.* **27**, 47 (1979).
[34]P. S. Steif, F. Spaepen, and J. W. Hutchinson, Acta Metall. **30**, 447 (1982).
[35]H. G. E. Hentschel, S. Karmakar, E. Lerner, and I. Procaccia, Phys. Rev. Lett. **104**, 025501 (2010).
[36]F. Spaepen, Scr. Mater. **54**, 363 (2006).
[37]A. Christiansen and J. B. Shortall, J. Mater. Sci. **11**, 1113 (1976).
[38]J. J. Lewandowski, W. H. Wang, and A. L. Greer, Philos. Mag. Lett. **85**, 77 (2005).
[39]X. Mao and T. Shoji, J. Mater. Sci. **28**, 927 (1993).
[40]A. Mattoni, L. Colombo, and F. Cleri, Phys. Rev. Lett. **95**, 115501 (2005).
[41]S. Mukherjee, W. L. Johnson, and W. K. Rhim, Appl. Phys. Lett. **86**, 014104 (2005).
[42]T. Iida and R. I. L. Guthrie, *The Physical Properties of Liquid Metals* (Clarendon, Oxford, 1988), p. 134.
[43]C. C. Yuan and X. K. Xi *et al.* (unpublished).
[44]D. H. Bae, S. W. Lee, J. W. Kwon, S. Yi, and J. S. Park, J. Mater. Res. **21**, 1305 (2006).
[45]A. H. Brothers and D. C. Dunand, Adv. Mater. **17**, 484 (2005).
[46]D. C. Hofmann, J. Y. Suh, A. Wiest, G. Duan, M. L. Lind, M. D. Demetriou, and W. L. Johnson, Nature (London) **451**, 1085 (2008).
[47]S. Pauly, S. Gorantla, G. Wang, U. Kuhn, and J. Eckert, Nature Mater. **9**, 473 (2010).
[48]P. A. Johnson, H. Savage, M. Knuth, J. Gomberg, and C. Marone, Nature (London) **451**, 57 (2008).